ChemPubSoc Europe

DOI: 10.1002/chem.201503102

CHEMISTRY
A European Journal
Full Paper

Single-Molecule Magnets

Role of Magnetic Exchange Interactions in the Magnetization Relaxation of {3d–4f} Single-Molecule Magnets: A Theoretical Perspective

Saurabh Kumar Singh, Mohammad Faizan Beg, and Gopalan Rajaraman*[a]

Abstract: Combined density functional and ab initio calculations are performed on two isomorphous tetranuclear $\{Ni_3^{III}Ln^{III}\}$ star-type complexes [Ln = Gd (**1**), Dy (**2**)] to shed light on the mechanism of magnetic exchange in **1** and the origin of the slow magnetization relaxation in complex **2**. DFT calculations correctly reproduce the sign and magnitude of the *J* values compared to the experiments for complex **1**. Acute ∢Ni–O–Gd bond angles present in **1** instigate a significant interaction between the $4f_{xyz}$ orbital of the Gd^{III} ion and $3d_{x^2-y^2}$ orbital of the Ni^{II} ions, leading to rare and strong antiferromagnetic Ni···Gd interactions. Calculations reveal the presence of a strong next-nearest-neighbour Ni···Ni antiferromagnetic interaction in complex **1** leading to spin frustration behavior. CASSCF + RASSI-SO calculations performed on complex **2** suggest that the octahedral environment around the Dy^{III} ion is neither strong enough to stabilize the $m_J \mid \pm 15/2\rangle$ as the ground state nor able to achieve a large ground-state–first-excited-state gap. The ground-state Kramers doublet for the Dy^{III} ion is found to be the $m_J \mid \pm 13/2\rangle$ state with a significant transverse anisotropy, leading to very strong quantum tunneling of magnetization (QTM). Using the POLY_ANISO program, we have extracted the J_{NiDy} interaction as $-1.45\ cm^{-1}$. The strong Ni···Dy and next-nearest-neighbour Ni···Ni interactions are found to quench the QTM to a certain extent, resulting in zero-field SMM behavior for complex **2**. The absence of any ac signals at zero field for the structurally similar $[Dy(AlMe_4)_3]$ highlights the importance of both the Ni···Dy and the Ni···Ni interactions in the magnetization relaxation of complex **2**. To the best of our knowledge, this is the first time that the roles of both the Ni···Dy and Ni···Ni interactions in magnetization relaxation of a {3d–4f} molecular magnet have been established.

Introduction

Single-molecule magnets (SMMs) are molecules that retain their magnetization even after the removal of the magnetic field, and display slow relaxation of magnetization owing to an intrinsic barrier for spin-reversal.[1] Indeed, if the relaxation is very slow, these SMMs show a hysteresis loop of purely molecular origin, very similar to classical bulk magnets. The presence of such features suggests a wide range of potential applications in such as high-density information storage devices, quantum computing, and molecular spintronics.[2] Enormous efforts have been made in the past two decades to improve the barrier height for the magnetization reversal, and hence, the blocking temperatures (T_B) to exploit these properties for practical applications.[1b,3] Several experimental and theoretical reports suggest that the presence of highly anisotropic ions in the cluster aggregation offers a large magnetic anisotropy in the ground state, which results in longer relaxation times. In this regard, highly anisotropic lanthanide ions are found to be promising for building SMMs, because they possess large magnetic anisotropy owing to unquenched orbital angular momentum associated with deeply seated 4f electrons holding negligible ligand field effects. This results in the isolation of several mononuclear and polynuclear complexes displaying energy barriers for spin-reversal as high as 938 K,[4] which is more than an order of magnitude higher than those displayed by the iconic $[Mn_{12}Ac]$ complex. Despite possessing such a large energy barrier for spin-reversal, the presence of multiple relaxation pathways, in particular, the significant quantum tunneling of magnetization (QTM) process, offers a shortcut for spin-reversal, which drastically reduces the relaxation time and diminishes the blocking temperature in almost all the lanthanide-based complexes. Due to this reason, the T_B values reported for all the lanthanide complexes are only marginally higher than that of the transition metal complexes.[3a,4b] In the literature, it has already been reported that the presence of stronger exchange interactions quenches QTM and prevents the loss of magnetization even in zero field.[5] Several strategies have been reported to enhance the magnetic coupling in lanthanide complexes. One of these includes the combination of lanthanide ions with radicals, which offers a strong magnetic exchange, and hence, quenches the QTM process significantly. An elegant example in this category is the $[\{[(Me_3Si)_2N]_2Ln(THF)\}_2(\mu\text{-}\eta^2\text{:}\eta^2\text{-}N_2)]$ complex (Ln = Dy, Tb), which possesses large thermal energy barriers [376 K (Tb) and 177 K

[a] Dr. S. K. Singh, M. F. Beg, Prof. Dr. G. Rajaraman
Department of Chemistry
Indian Institute of Technology Bombay
Powai, Mumbai, 400076 (India)
E-mail: rajaraman@chem.iitb.ac.in

Supporting information for this article is available on the WWW under http://dx.doi.org/10.1002/chem.201503102.

(Dy)] and record blocking temperatures [14 K (Tb) and 8.3 K (Dy)] for magnetic relaxation.[6] Theoretical studies suggest that the diffused magnetic orbitals of the N_2^{3-} interact directly with the 4f orbitals of the lanthanide ions, leading to a very large magnetic exchange interaction.[7] However, stronger lanthanide–radical interactions demand localization of the radical character; these conditions are often difficult to meet as this is directly correlated with the stability of the complexes under ambient conditions.[8]

An alternative strategy is to isolate the mixed transition metal and lanthanide-based complexes, where the strength of the magnetic exchange is found to be significantly stronger than in the pure lanthanide-based complexes.[3b] Langley et al. recently employed this strategy and reported a tetranuclear $\{Cr_2Dy_2\}$ complex possessing a very large J_{DyCr} exchange (as high as $-20\ cm^{-1}$; with a projected pseudo-spin $^1/_2$) leading to a slow relaxation of magnetization and with a hysteretic behavior below 3.5 K.[9] Recently, Liu et al. reported a trinuclear $\{Fe_2Dy\}$ complex possessing a record barrier height of $319\ cm^{-1}$.[10] Exploiting this strategy, several polynuclear {3d–4f} complexes have been reported in the literature with attractive barrier heights.[9,11,12]

In addition to experiments, computational tools also play a pivotal role in understanding the magnetic properties of these classes of complexes. The increased power of quantum chemistry allows accurate estimation of nontrivial spin-Hamiltonian (SH) parameters such as magnetic anisotropy of transition metal ions and lanthanide ions, crystal field parameters of lanthanides, and isotropic/anisotropic/antisymmetric magnetic exchange parameters.[13] Combined density functional theory (DFT) and ab initio approaches have been employed successfully for the accurate derivation of such intricate parameters,[9,10] and at the same time, several successful predictions have also been made to achieve better SMMs.[14] In general, 3d···Gd interactions are ferromagnetic in nature; exploiting these features, several polynuclear {3d–4f} complexes are synthesized in which 3d···3d interactions are deliberately avoided. Classical examples in this category include trinuclear {3d–4f–3d} complexes,[12a,15] several of which are reported to be SMMs. Another elegant example is star-shaped complexes in which Ln^{III} ions are placed at the center of the triangle and each corner is occupied by a transition metal ion. In this category, $\{Ni_3Ln\}$, $\{Mn_3Ln\}$, and $\{Fe_3Ln\}$ clusters have been reported.[16] Besides tetranuclear complexes, there are also other larger clusters in which 3d···3d interactions are deliberately avoided.[17]

Previously, we have studied a series of {Ni-Gd} binuclear and {Ni-Gd-Ni} trinuclear complexes, using DFT methods[14c] to understand the mechanism of magnetic exchange and to develop magnetostructural correlations; later, this was extended to larger {3d-Gd} clusters.[18] As the magnetic exchange interaction has been found to have a tremendous influence on the magnetization relaxation, here we decided to undertake a detailed theoretical study on structurally similar $\{Ni_3Gd\}$ and $\{Ni_3Dy\}$ complexes. For this purpose, we chose star-shaped $[Ni_3Ln\{(py)_2C(H)O\}_6](ClO_4)_3$ complexes [Ln = Gd (**1**), Dy (**2**), and $(py)_2C(H)O^-$ is the anion of di-2-pyridylmethanol].[16a] Magnetic studies reveal that the Ni···Gd magnetic exchange interaction present in complex **1** is antiferromagnetic in nature ($J_{NiGd} = -1.09\ cm^{-1}$ and $J_{NiNi} = -0.99\ cm^{-1}$) and complex **2** is characterized as an SMM at zero field, albeit with a very small barrier height. Solid proof of SMM characteristics of complex **2** comes from single-crystal magnetization studies, which show a hysteresis loop below 0.2 K. By modelling these two complexes, we would like to answer the following key questions: 1) Why are the Ni···Gd interactions found in complex **1** antiferromagnetic in nature, whereas the majority of reported Ni···Gd interactions are ferromagnetic? 2) What is the origin of the strong 1,3 Ni···Ni interactions present in complex **1**? 3) How does the magnetic exchange interaction influence the magnetic relaxation and is there a way to improve the barrier height in complex **2**?

Computational Details

In complex **1**, to extract the magnetic coupling between the Ni^{II}–Gd^{III} ions and the 1,3 Ni^{II}–Ni^{II} interactions, we employed the pairwise interaction model.[19] We computed seven spin configurations (J_1–J_6; see Supporting Information for details) to extract all six J values. The energy difference between the spin configurations is equated to the corresponding pairwise interaction to extract the J values. The Hamiltonian shown in Equation (1) is used to describe the isotropic magnetic exchange interaction in complex **1**.

$$\hat{H} = -J_1\hat{S}_{Ni1}\hat{S}_{Gd} - J_2\hat{S}_{Ni2}\hat{S}_{Gd} - J_3\hat{S}_{Ni3}\hat{S}_{Gd} - J_4\hat{S}_{Ni1}\hat{S}_{Ni2} - J_5\hat{S}_{Ni1}\hat{S}_{Ni3} - J_6\hat{S}_{Ni2}\hat{S}_{Ni3} \quad (1)$$

DFT in combination with the broken-symmetry (BS) approach[20] has been employed widely to extract spin-configuration energies. The BS approach has an excellent track record of yielding good numerical estimates of J values in a variety of complexes.[18,19,21,22] Here, all the DFT calculations are performed with the Gaussian 09 suite of programs.[23] We used the hybrid B3LYP functional[24] along with the double-ζ relativistic effective core potential CSDZ basis set for Gd,[25] Ahlrichs triple-ζ TZV basis set for Ni,[26] and 6-31G* for the other atoms.[27] Our earlier findings suggest that the combination of the B3LYP functional with the aforementioned basis sets yield good numerical estimates of J values in {3d-Gd} complexes.[14c,18,21i,28] A tight convergence ($1\times10^{-8}\ E_h$) was employed for all the calculations.

High-level ab initio calculations were employed to compute the single-ion anisotropies of the Ni^{II} and Dy^{III} centers. All these calculations were performed using the MOLCAS 8.0 suite of programs.[29] Basis sets describing all the atoms were taken from the ANO-RCC library available in the MOLCAS package. Here, we employed the [ANO-RCC..8s7p5d3f2g1h.] basis set for Dy atoms, [ANO-RCC..6s5p3d2f1g.] basis set for Ni atoms, [ANO-RCC..3s2p1d] basis set for C, N, and O atoms, and [ANO-RCC..2s] basis set for H atoms. The ground-state configuration for the Dy^{III} ion is $4f^9$, and the corresponding atomic multiplet is $^6H_{15/2}$. First, we performed CASSCF calculations, which comprise an active space of nine active electrons in seven active 4f orbitals, denoted as CAS(9,7). We computed 21 sextet states (^6H, ^6P, ^6F) in the CI procedure, as these states are found to be precise enough to reproduce the low-lying energy spectrum as well as the g-tensor values.[14b,30] Subsequently, we mixed all these 21 sextets in the RASSI-SO module to compute the spin-orbit states (see Supporting Information for details). We have not incorporated the dynamic correlation effects by the mean of

CASPT2 calculations due to the hardware limitations. However in our earlier studies, we have shown that the incorporation of dynamic correlation have minimal effects on the computed low-lying energy pattern and g-tensors.[31] Furthermore, we took these computed SO states in the SINGLE_ANISO program[32] to compute the g-tensors of eight low-lying Kramers doublets (KDs). For the Ni^{II} centers, the active space comprises eight active electrons in five active metal-based d-orbitals, that is, a CAS(8,5) setup. Here, we computed 10 triplets and 15 singlets in the CI procedure, and later, we mixed all these states in the RASSI-SO module to compute the spin-orbit states. In a similar fashion, we introduced these SO states in the SINGLE_ANISO module[13b,33] to compute the g-tensors for each of the Ni^{II} centers. The Cholesky decomposition for two-electron integrals was used to save disk space. The magnetic exchanges between the Ni^{II} and Dy^{III} were extracted by using Lines' model,[34] which requires the computed ab initio energies and the wavefunction of the corresponding Ni^{II} and Dy^{III} ions. In general, nine exchange parameters are required to extract the anisotropic exchange for pseudo spins $\tilde{S}=1/2$ of Kramers doublets of two metal sites. The main advantage of Lines' model is that it requires only one parameter (J) to simulate the anisotropic exchange coupling for each pair. In this model, the isotropic exchange part between two given pairs of metals, assuming no spin-orbit interactions, is first modelled by a single-parameter Heisenberg exchange Hamiltonian. In the next step, it diagonalizes the matrix of this Hamiltonian on the basis of the obtained spin-orbit multiplets for each metal fragment, and provides a solution corresponding to anisotropic exchange between the Kramers doublet. Moreover, this model has been found to be exact in the limits of two fully isotropic ions, two Ising-type ions, or one Ising and one isotropic ion. Here, we extracted the magnetic exchange interaction for which Ni^{II} is isotropic whereas the Dy^{III} ion is of Ising type. All these simulations were performed using the POLY_ANISO code developed by Chibotaru and co-workers to extract the Ni···Dy magnetic exchange interaction in complex **2**.[13b,33] This code has been used routinely to extract the magnetic exchange, to obtain the exchange spectrum, and temperature- and field-dependent magnetic properties in these classes of complexes.

Results and Discussion

Theoretical studies on complex 1

X-ray structural analysis reveals that both complexes **1** and **2** are isomorphous, where all the three Ni(II) ions and Ln(III) ion are arranged in the centred triangular plane. The Ln(III) ion lies at the centre of the near-equilateral triangle, while Ni(II) ions occupy the corners of the triangle. Both the Ln^{III} and Ni^{II} ions are in the distorted hexa-coordination environment. The central Ln^{III} is bound by the deprotonated O atoms of the six $\eta^1{:}\eta^1{:}\eta^1{:}\mu$-$(py)_2C(H)O^-$ groups, each serving as a bridge between the Ni^{II} and Ln^{III} ions. These complexes possess a propeller shape with pseudo D_3 symmetry. Examination of structural parameters suggests that out of the three Ni^{II} centers, two Ni^{II} (namely Ni1 and Ni2) centers are almost identical, and the third (Ni3) center is slightly distorted (see Tables S1, S2, Supporting Information, for crystal structure and ChSm details).

Because of minor differences observed in the ∢Ni–O–Gd bond angles, ∢O–Ni–O–Gd dihedral angles, and out-of-plane parameter (τ), we have assumed six different J' values in **1** to model the magnetic data (see Table S1, Supporting Information). The crystal structure of complex **1** along with the adapted exchange scheme is depicted in Figure 1. The experimental magnetic susceptibility collected at 0.1 T field in the range 5.0–300 K yields an antiferromagnetic exchange for both com-

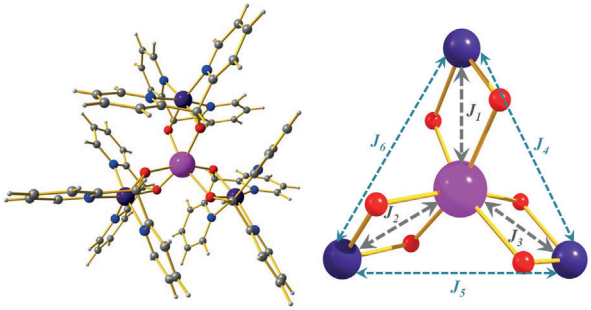

Figure 1. X-ray crystal structure of complex **1**[16a] (left); employed exchange scheme for complex **1** (right). Color code: Gd (pink), Ni (violet), N (blue), O (red), C (gray), H (white).

plexes **1** and **2**. The best fit to the susceptibility data for complex **1** yields a J_{NiGd} value (assuming all three J_{NiGd} interactions are the same) of $-1.09\ cm^{-1}$ with similar J_{NiNi} 1,3 interactions ($-0.99\ cm^{-1}$).[16a] DFT calculations were performed on complex **1** without any structural modifications, and the computed J values are -1.32, -1.31, -1.67, -0.32, -0.29, and $-0.56\ cm^{-1}$ for J_1–J_6, respectively. Our computed J values nicely reproduce the sign of both the J_{NiGd} and J_{NiNi} values obtained experimentally; however, the magnitudes of the J_{NiNi} interactions are underestimated. The computed energies of all the spin states along with $<S^2>$ values are provided in Table S3 (Supporting Information). To further crosscheck our computed values, we have carried out calculations on model complexes using diamagnetic substitution methods. Here, we prepared three model complexes by substituting two of the Ni^{II} ions with Zn^{II} analogues, and performed calculations assuming a dinuclear Ni^{II} and Gd^{III} complex. Calculations on these three model complexes yield J values of -1.43, -1.49, and $-1.89\ cm^{-1}$ for J_1, J_2, and J_3 interactions, respectively (see Table S5, Supporting Information, for details). Both methods, although yielding very similar J_{NiGd} interactions, as the Ni3 center is slightly distorted compared to the other two centers, the J_3 interaction is found to deviate significantly from the J_1 and J_2 values. Similarly, the J_4 and J_5 interactions associated with the Ni3 center are found to deviate from the J_6 interaction. The computed J values nicely reproduce the experimental magnetic susceptibility data, which increases confidence in the estimated J values (see Figure S4, Supporting Information).

In general, the {Ni–Gd} interactions are found to be ferromagnetic in nature with only a few exceptions.[16a,35] Interestingly, in complex **1**, the Ni···Gd interactions are found to be antiferromagnetic in nature (the strongest antiferromagnetic interaction known for any {Ni-Gd} complexes); to understand the reason behind this observation, we probed the mechanism of the magnetic exchange for this pair. For this pair, the net exchange interaction has two contributions: ferromagnetic (J_F)

and antiferromagnetic (J_{AF}) interactions, with the net J value given in Equation (2).

$$J = J_F + J_{AF} \quad (2)$$

The J_F contribution arises from the interaction of the Ni^{II} magnetic orbitals with the empty 5d Gd^{III} orbitals. On the other hand, the J_{AF} contribution arises solely because of the overlap between the 3d orbitals of Ni^{II} and 4f orbitals of Gd^{III} ions. The dominating part decides the sign of the net J value. The importance of these contributions has already been highlighted in our earlier extensive studies on {Ni-Gd} complexes.[14c] In the majority of complexes, the J_F term dominates because the 4f orbitals are inert in nature and do not interact significantly with the Ni^{II} orbitals, leading to ferromagnetic Js. However, this is strongly dependent on the structure, as larger ∢Ni–O–Gd angles favor the J_F term, whereas acute ∢Ni–O–Gd angles favor the J_{AF} term. To gain insights into the J_F contributions, we analyzed the NBO populations. Acute ∢Ni–O–Gd angles present in **1** lead to less efficient charge transfer from the Ni^{II} to the Gd^{III} ion, and therefore, relatively smaller occupations of 5d orbitals are detected at the Gd^{III} center. To gain insight into the J_{AF} contribution, we computed the overlap integral between the Ni^{II} and Gd^{III} ions. Overlap integral analysis was performed on diamagnetic substituted models. There are 14 possible interactions for a {Ni-Gd} pair, four of which are found to be significant for all three interactions (J_1–J_3). In particular, the interaction between the $4f_{xyz}$ orbitals of Gd^{III} and $3d_{x^2-y^2}$ orbitals of Ni^{II} are found to be very strong, leading to a dominant J_{AF} interaction and net antiferromagnetic J in **1** (see Figure 2 right). In addition, the trend of J_3 being larger than J_1 and J_2 is also reflected in the computed overlap integrals (for details, see Table S6 and Figure S3, Supporting Information)

The computed spin density plot for the high spin state of complex **1** is shown in Figure 2. The spin density on the Gd^{III} ion (7.01) reflects a weak polarization around the Gd^{III} ion. The spin density of 1.56 found on the Ni^{II} ions and significant spin densities (≈0.75) on the bridging ligand suggest strong delocalization of spins from the Ni^{II} ions (see Table S4 and Figure S2, Supporting Information). As Gd^{III} and Ni^{II} ions promote different mechanisms, a mixture of spin polarization and spin delocalization mechanisms is operational here for the magnetic coupling.

To gain more insight into the magnetic coupling, we analyzed the structural parameters in detail. The ∢Ni–O–Gd bond angle is found to govern the sign as well as the magnitude of the J value, with a smaller angle leading to antiferromagnetic coupling and a larger angle yielding ferromagnetic coupling. Here, we note that the out-of-plane shift (defined as parameter τ)[19] of the alkyl groups attached to the μ-oxo bridges in conjunction with a smaller ∢Ni–O–Gd angle can also influence the Ni···Gd interactions. Here, the ∢Ni–O–Gd angles are found to be 94° and 95° for J_3 and J_1–J_2 interactions, respectively. These angles are much smaller than those observed for binuclear {Ni-Gd} complexes, and reflect our earlier observations.[14c] Moreover, the fact that J_3 is larger than J_1–J_2 interactions can also be rationalized on the basis of the relative ∢Ni–O–Gd bond angles. The 1,3 Ni···Ni interactions occur through space, and are generally found to be very weak in nature (in the range 0.01–0.5 cm^{-1}). Here, however, these interactions are stronger owing to the shorter Ni^{II}···Ni^{II} distances (≈5.5 Å) observed.

Our calculations predict a ground state of $S=1/2$ for complex **1**, followed by an $S=3/2$ state at 4.3 cm^{-1} and two degenerate $S=3/2$ states at 10.5 cm^{-1}. Here, the Ni···Gd and the 1,3 Ni···Ni interactions are competing with each other, leading to a spin frustration. However, the $S=1/2$ state is uniquely defined, arising from spin-up on Gd^{III} and spin-down on three Ni^{II} centers; these competing interactions result in three nested $S=3/2$ first excited states. To understand the energy levels in detail, we varied the J_{NiGd}/J_{NiNi} ratio and plotted the Eigen values of all the spin states from the ground state that lie within an energy window of 40 cm^{-1} (see Figure 3b). For a J_{NiGd}/J_{NiNi} ratio of 1.0, this results in complete spin frustration: the ground state is still $S=1/2$ but all the excited states are degenerate. For a ratio $J_{NiGd}/J_{NiNi}<1$, the ground-state spin values vary from $S=1/2$ to $S=7/2$. At a J_{NiGd}/J_{NiNi} ratio of 0.66, the ground state $S=1/2$ switches to $S=3/2$ as the ground state.

Further lowering the ratio of J_{NiGd}/J_{NiNi} below 0.44 leads to stabilization of $S=5/2$ as the ground state, and at values below 0.22, for which the J_{NiNi} interaction dominates, the resul-

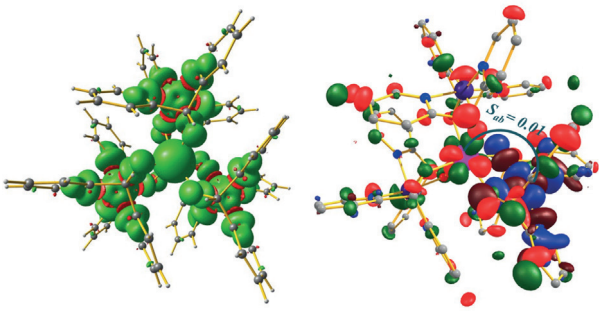

Figure 2. DFT-computed spin density plot of complex **1** for $S=13/2$ state (left). The isodensity surface represented here corresponds to a value of 0.005 e^{-} $bohr^{-3}$. The green and red regions represent the positive and negative spin densities, respectively. The strongest interaction is observed between the $4f_{xyz}$ orbital and $d_{x^2-y^2}$ orbital of Ni^{II} (right). For a better visualization we have kept the surfaces in two different colors.

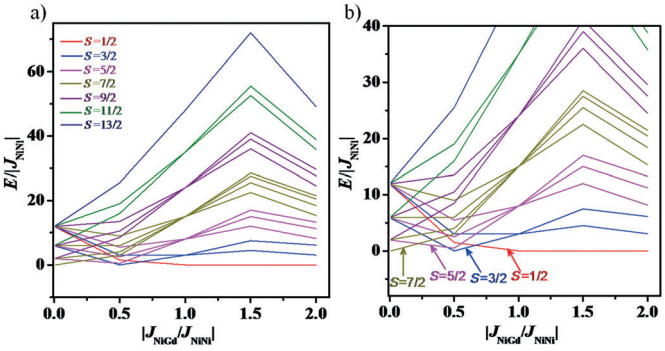

Figure 3. a) Plot of calculated Eigenvalues versus J_{NiGd}/J_{NiNi} for complex **1**; b) the same diagram plotted with an energy scale of 40 cm^{-1} on the y axis.

tant ground state is found to be the $S=7/2$ state (essentially complete spin frustration between three Ni^{II} leading to the $S=0$ state and uncoupled Gd^{III} leading to stabilization of the $S=7/2$ state). For the DFT calculated values, the J_{NiGd}/J_{NiNi} ratio is found to be 3.6, suggesting the presence of the $S=1/2$ ground state. It is evident from the plot that for $J_{NiGd}/J_{NiNi}<1$, the energy levels are low-lying, and the fact that both the ground state and the excited states depend strongly on the ratio of J_{NiGd}/J_{NiNi} suggests that there is a degree of frustration in complex **1**. For $J_{NiGd}/J_{NiNi}>1$, the degree of spin frustration is minimal, and the ground state is suggested as $S=1/2$, which can be accounted for by simple pairwise exchange interactions. However, for $J_{NiGd}/J_{NiNi}<1$, spin frustration will cause the net alignment of the spin vector, so the simple pairwise exchange interaction model cannot be employed, as the ground state is determined by the degree of spin frustration.

Theoretical studies on complex 2

In this section, we have tried to analyze the origin of magnetic anisotropy in complex **2**, and have placed our emphasis on the single-ion anisotropy of the three Ni^{II} ions and the central Dy^{III} ion, and how the coupling between them leads to a blockade barrier. The coordination environments around the Ni^{II} ions in **2** are close to ideal octahedral structures, and thus, are unlikely to possess significant anisotropy, as we showed earlier in the NiN_4O_2 class of complexes (see Table S2, Supporting Information).[36] We have computed the anisotropy of the individual Ni^{II} ions using $\{NiZn_2Lu\}$ model complexes. The CASSCF computed spin-free energies, spin-orbit energies, and associated g-tensors and D-tensors for all three Ni^{II} centers are provided in Table S7, and their orientations are plotted in Figure S5 (Supporting Information). All three Ni^{II} ions exhibit only a small zero-field splitting parameter, as expected ($D\approx 4\ cm^{-1}$). The positive nature of the D values and relatively small magnitude observed suggest that the Ni^{II} ion lacks significant anisotropy, and are unlikely to be the reason for the blockade of magnetization in **2**.

To compute the single-ion anisotropy of the Dy^{III} ion, we have substituted all three Ni^{II} ions with their diamagnetic Zn^{II} analogues. The central Dy^{III} ion possesses a distorted octahedral geometry (the deviation being 1.904, as indicated by ChSm analysis,[37] see Table S2). The $4f^9$ Dy^{III} ion is a Kramer ion possessing the ground-state term $^6H_{15/2}$. The ab initio computed low-lying energy spectrum of complex **2** is spanned over an energy range of 680 cm^{-1}, and the computed g-tensors for the eight low-lying KDs are provided in Table 1 and Table S8 (Supporting Information). The computed values are broadly in agreement with the g-values reported for other six-coordinate Dy^{III} complexes.[38] The g-tensors of the ground-state KDs are axial in nature ($g_{xx}=0.8082$, $g_{yy}=0.9278$, and $g_{zz}=16.9163$), but depart significantly from the pure Ising-type anisotropy generally preferred for SMMs ($g_{xx}=g_{yy}=0$; $g_{zz}=20$). The wavefunction analysis suggests that the ground-state wavefunction is mainly $|\pm 13/2\rangle$: $0.90|\pm 13/2\rangle+0.29|\pm 15/2\rangle+0.19|\pm 7/2\rangle$ with a significant mixing with the other subsequent excited states (see Table S9 for details). The principal magnetic axis of the ground-state KD is found to lie along the pseudo C_3 symmetric axis (deviates by $\approx 8.2^\circ$) perpendicular to the triangle plane. This orientation is in accordance with the minimum electrostatic repulsion and the highest-order rotational symmetry conditions.[39]

Table 1. CASSCF + RASSI-SO calculated energies of eight low-lying KDs, the g-tensors associated with each KD, along with deviation from the principal magnetization axis of the ground-state KD.

J multiplet	Spin-orbit energies [cm^{-1}]	g_{xx}	g_{yy}	g_{zz}	θ
$^6H_{15/2}$	0	0.8082	0.9278	16.9163	–
	16.59	0.7251	0.8910	14.1075	16.8
	114.79	0.0530	0.0740	11.3177	8.1
	166.10	0.0246	0.0295	19.6177	9.1
	268.11	4.2351	4.3686	7.8110	9.6
	457.42	3.8781	4.3787	5.1334	6.7
	596.24	0.9996	1.9241	4.7467	3.9
	680.66	11.9925	8.6738	1.0715	7.2

The first excited KD is found to lie 16.5 cm^{-1} higher in energy from the ground-state KD, and is mainly $m_J\ |\pm 11/2\rangle$ state. This state, however, is found to mix strongly with other m_J levels. The observed g-tensors for the first excited KD are $g_{xx}=0.7251$, $g_{yy}=0.8910$, and $g_{zz}=14.1075$, suggesting a significant transverse component. The orientation of the main magnetic axis of the first excited KD is also found to lie along the pseudo C_3 axis with a tilt of 16.8° from the ground-state KD (see Figure 4). This suggests that the relaxation is expected to occur via the first excited state, which is only around 16 cm^{-1} higher in energy (vide infra).

We have also computed the crystal field parameters to analyze the QTM between the ground-state KDs. The computed crystal field parameters show that the nonaxial terms B_k^q ($q\neq 0$, and $k=2, 4, 6$) terms are larger than the axial terms ($q=0$, and $k=2, 4, 6$), resulting in a large transverse magnetic anisotropy in the ground-state KD. However, quite large values of the nonaxial B_2^{-1}, B_2^{-2}, B_4^{-1}, and B_2^{-4} terms induce significant mixing between all components of the ground $m_J=15/2$ manifold (see Table S10 for details). As a result, the ground doublet state acquires significant transverse anisotropy ($g_{xx}=0.8082$, $g_{yy}=0.9278$). The presence of significant nonaxial terms alongside large values of g_{xx}/g_{yy} suggests that QTM in the ground state is operative along with TA-QTM via the first excited state.

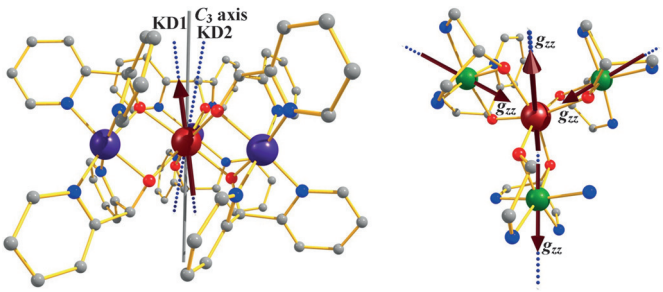

Figure 4. Ab initio computed orientation of the principal magnetization axes of the ground and first excited KDs along with pseudo C_3 axis (left). Ab initio computed main magnetic axes of the Dy^{III} and three Ni^{II} centers (right).

The orientation of the g-tensors (using pseudo-spin 1/2) for all the three Ni^{II} centers are found to be directed towards the pseudo C_2 axes passing through each Ni^{II}-Dy^{III} axis (see Figure 4), whereas the main anisotropy axis of the Dy^{III} ion lies perpendicular to the C_2 axis (along the pseudo C_3 axis).

Calculations suggest that the distorted octahedral ligand field around the Dy^{III} ion present in **2** is neither significant enough to enhance the gap between the ground and first excited KD nor stabilizes the desired $m_J \mid \pm 15/2\rangle$ as the ground state. This clearly implies that if the relaxation is single-ion in origin, complex **2** is unlikely to exhibit zero-field SMM behavior. This is supported by the fact that the structurally similar, octahedral Dy^{III} ion in the $[Dy(AlMe_4)_3]$ complex exhibits very fast magnetic relaxation even in the presence of an applied field.[38] At zero field, it does not exhibit any SMM characteristics, suggesting significant QTM in this complex.

Ab initio calculations suggest that neither the magnetic anisotropy of Ni^{II} ions nor that of the Dy^{III} ion alone is sufficient to rationalize the observed magnetization blockade in complex **2**. Thus, the slow relaxation observed in zero field for this complex is expected to be governed mainly by the exchange-coupled states arising from the Ni···Dy and Ni···Ni interactions.

To obtain an estimate of the J_{NiDy} interaction, we simulated the magnetic susceptibility data using Lines' model in the POLY_ANISO program. To estimate the J_{NiDy} exchange, the 1,3 Ni···Ni interactions are fixed at $-0.39\ cm^{-1}$ (average of J_4–J_6 interactions computed for complex **1**) and it is assumed that all three Ni···Dy interactions are the same (that is, $J_1 = J_2 = J_3$ scenario compared to complex **1**) to avoid over-parameterization in fitting featureless susceptibility data. In employing Lines' model, we have mixed the low-lying (below $100\ cm^{-1}$ energy) spin-orbit states of the Dy^{III} ion with the low-lying energy states of three Ni^{II} ions computed using CASSCF calculations. The spectrum of the lowest spin-orbit exchange multiplets of complex **2** corresponding to the fitted exchange parameters consists of 108 exchange states, grouped in 54 KDs. The 54 KDs arises from two KDs of Dy^{III} ($<100\ cm^{-1}$) and three spin functions of each $S = 1$ Ni^{II} center ($2\times3\times3\times3$; see Figure S7, Supporting Information). From Table 1 it is evident that the ground-state KD of the Dy^{III} ion is not axial in nature and the first excited state is low-lying in energy ($<20\ cm^{-1}$); this implies that the nature of the Ni···Dy exchange will not be the pure Ising type. Simulation of the susceptibility data (from 1.8 to 50 K) yields J_{NiDy} as $-1.45\ cm^{-1}$ (see Figure S6, Supporting Information). The obtained value of J_{NiDy} suggests a strong antiferromagnetic coupling between the Dy^{III} and Ni^{II} ions, and is similar in magnitude to the estimate obtained for complex **1**. To check the validity of the exchange coupling obtained from the fitting, we rescaled the average J_{NiGd} obtained for complex **1** for the Ni···Dy interaction; this yields J_{NiDy} as $-1.01\ cm^{-1}$.[9] These independent methods of extracting J values adds confidence in the estimated parameter. The low-lying 54 exchange-coupled states computed for complex **2** are arranged according to the values of their magnetic moments in Figure 5b (see also Figure S7, Supporting Information).[12a,40]

The absolute energies of the low-lying exchange doublets as well as the corresponding g-tensors are listed in Table S11 (Supporting Information). From Figure 5b, it is evident that the exchange-coupled states are arranged in a trend in which the gap between the first and second KDs is approximately $2\ cm^{-1}$, and this is followed by nearly degenerate third and fourth excited KDs, that is, there are three nearly degenerate first excited states. This reveals that the first excited exchange doublets are non-Ising type, as the first excited KD is mixed strongly with the nearly degenerate third and fourth excited KDs. This nested arrangement of energy levels observed in complex **2** is very similar to the spin-state arrangement estimated for complex **1**, suggesting that spin frustration/competing interactions open up several relaxation channels at the first excited state level.

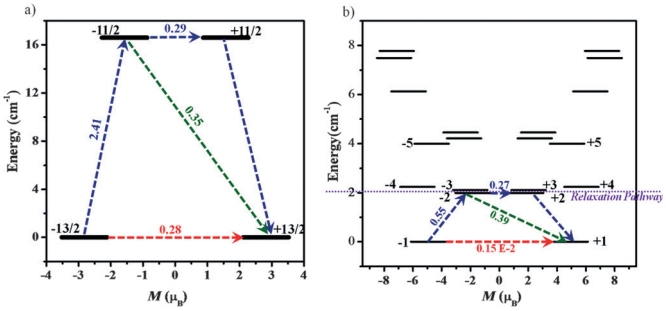

Figure 5. Ab initio computed magnetization blocking barrier for a) single-ion Dy(III) and b) for exchange-coupled complex **2**. Thick black line indicates KDs as a function of magnetic moment. Dotted green lines show the possible pathway of the Orbach process. Dotted blue lines show the most probable relaxation pathways for magnetization reversal. Dotted red lines represent the presence of QTM between the connecting pairs. The numbers provided at each arrow are the mean absolute values for the corresponding matrix element of the transition magnetic moment.

The anisotropy for the ground-state KD is found to be axial in nature ($g_{xx} = 0.003$, $g_{yy} = 0.006$ and $g_{zz} = 9.902$), and is oriented along the pseudo C_3 axis. The first excited exchange-coupled doublet is located $1.98\ cm^{-1}$ higher in energy with a significant transverse component ($g_{xx} = 0.175$, $g_{yy} = 1.11$, and $g_{zz} = 3.997$). The computed transverse magnetic moments between the ground state suggests that the quantum tunneling (QTM = $0.15\times10^{-2}\ \mu_B$) is relatively quenched compared with the single-ion behavior (QTM = $0.2\ \mu_B$; see Figure 5a). This is attributed to the presence of a strong J_{NiDy} exchange interaction; however, the quenching is not sufficient to suppress the tunneling completely (usually for exchange doublet states in which complete quenching is observed, the computed matrix elements are of the order of 10^{-6}–$10^{-10}\ \mu_B$). Single-crystal measurements performed on complex **2** reveal a hysteresis loop below 0.2 K; however, large relaxation at zero field was observed, and this is attributed to the QTM effects. Our calculations strongly support this experimental observation.

The next probable pathway for the relaxation is thermally assisted QTM (TA-QTM) via the first excited state, which is found to be significant (TA-QTM = $0.27\ \mu_B$). This is essentially attributed to the fact that the first excited KD is strongly mixed with the nearly degenerate second and third excited KDs. This opens up a major relaxation pathway via the first excited KDs governed by TA-QTM/Orbach processes, and places the estima-

tion of barrier height at 1.98 cm^{-1}. The out-of-phase ac signals are observed only below 3 K for complex **2**; this estimates the barrier height to be roughly 2 cm^{-1}, which is in agreement with the calculated barrier height.Besides the J_{NiDy} exchange interaction, the 1,3 Ni···Ni interactions are also found to play a role in quenching the quantum tunneling of magnetization. This is affirmed by an additional simulation using the POLY_ANISO program with the 1,3 Ni···Ni interactions assumed to be zero. This additional simulation predicts a larger probability for QTM and TA-QTM processes. However, the competing nature of the J_{NiNi} and J_{NiDy} interactions lead to a mixed effect on the magnetic relaxation of complex **2**.

To analyze the impact of the structural distortion on the origin of magnetic anisotropy in the central Dy^{III} ion, we have developed a magnetostructural correlation in which we moved the Dy^{III} ion out of the triangular plane (see Figure 6 and Figure 6a inset). To perform this correlation, we tailored complex **2** to avoid steric interactions with bulky ligands (see model structure **2a**, Figure S8, Supporting Information).The computed gap between the ground state and first excited state KD for **2a** is estimated to be approximately 13.5 cm^{-1} (U_{cal}), with the g-values similar to those of complex **2**. As the Dy^{III} ion moves out of plane, the U_{cal} value increases gradually, reaching as high as 35 cm^{-1} for the most distorted structure (see Figure 6). However, a closer look at the estimate of the g-tensors reveals that the increase in the U_{cal} value is accompanied by an increase in transverse anisotropy, leading to an increase in QTM behavior between the ground-state KDs (see Table S12). Thus, our correlation suggests that for the Dy^{III} ion, octahedral coordination is unlikely to help enhance the magnetization blocking even with very strong distortion, and this is supported by earlier observations on real and model complexes.[14a,41]

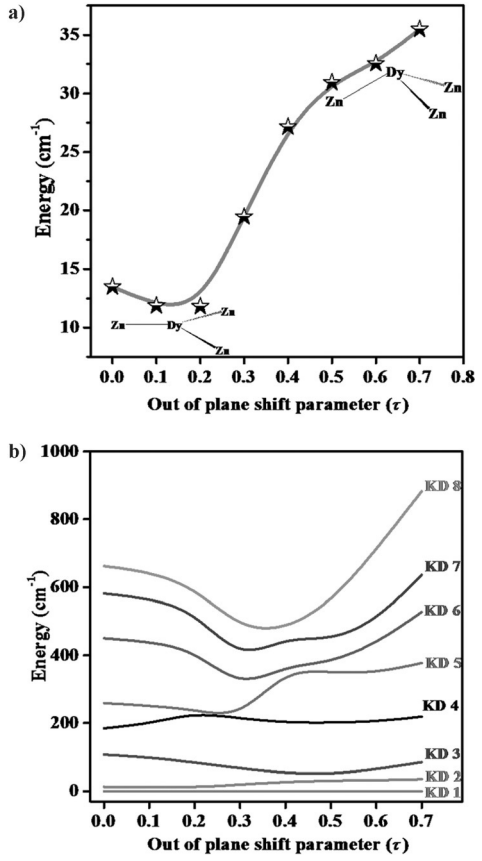

Figure 6. a) CASSCF + RASSI-SO computed gap between the ground state and first excited KD for the out-of-plane shift parameter. b) Behavior of eight low-lying KDs as a function of out-of-plane shift parameter (Å).

Conclusion

In summary, we have reported here a detailed computational investigation on two tetranuclear {Ni_3Ln} complexes (Ln = Gd, Dy) with the aim of analyzing the origin of the strong antiferromagnetic Ni···Gd interaction in **1** and to understand the role of the exchange interaction in the magnetization relaxation of complex **2**.

DFT calculations using the B3LYP functional yielded a good numerical estimate of both the Ni···Gd and 1,3 Ni···Ni interactions compared with the experimental results, and the computed values reproduced the experimental susceptibility data nicely. Our calculations reveal that the strong antiferromagnetic Ni···Gd interaction arises because of acute ∢Ni–O–Gd bond angles, which curb the σ-type charge transfer from the 3d orbitals of the Ni^{II} ion to the vacant 5d orbitals of the Gd^{III} ion. Besides, the MO and overlap integral analysis suggested a relatively strong interaction between the $4f_{xyz}$ orbital of Gd^{III} and the $3d_{x^2-y^2}$ orbital of the Ni^{II} ion. This decisive overlap leads to strong antiferromagnetic J_{NiGd} values in complex **1**, and highlights the importance of the ∢Ni–O–Gd bond angle in determining the sign and strength of the *J* values.

For complex **2**, the single-ion anisotropy of the Dy^{III} ion was computed initially using the CASSCF + RASSI-SO approach. These calculations suggest that the presence of an octahedral ligand field leads to stabilization of m_J $|\pm 13/2>$ as the ground state with a significant transverse anisotropy. Besides, the excited-state KDs are found to be low-lying in energy, offering only a very small barrier for reorientation of magnetization. The ab initio computed blockade barrier revealed a significant QTM process between the ground states, and suggested that zero-field SMM properties are unlikely to be observed if the relaxation is purely single-ion in origin. This is supported by the fact that the [$Dy(AlMe_4)_3$] complex, in which the Dy^{III} ion is also found to be in octahedral coordination, does not show any SMM characteristics at zero field.

The simulation of the magnetic susceptibility of complex **2** using Lines' model revealed an antiferromagnetic exchange of −1.45 cm^{-1} between the Ni^{II} and Dy^{III} ions. The ab initio computed blockade barrier for exchange-coupled states suggested that the presence of a strong exchange interaction suppresses the QTM in the ground state compared with the QTM effect observed for the Dy^{III} single ion. Thus, the slow relaxation observed in complex **2** at zero field can be attributed to the exchange-coupled doublet state, and both the Ni···Dy and 1,3 Ni···Ni exchange interactions help suppress the QTM process to a certain extent.

Magnetostructural studies on the Dy^{III} single ion revealed that the out-of-plane shift parameter gradually increases the gap between the ground and first excited state KDs; however, the transverse component of the anisotropy was also found to increase at the same time, leading to an enhanced QTM process. Unfortunately, this advocates that octahedral Dy^{III} complexes are expected to exhibit no or very weak SMM behavior, even in the presence of strong exchange interactions. This highlights the importance of fine tuning of the single-ion anisotropy even in large {3d–4f} polynuclear complexes.

Acknowledgements

G.R. would like to acknowledge DST (EMR/2014/000247) and DST Nanomission (SR/NM/NS-1119/2011) for funding. G.R. acknowledges IITB for the High Performance Computing Facility. S.K.S. would like to thank the Department of Chemistry, IITB for a Research Associate position. We thank Dr. Liviu Ungur for providing the POLY_ANISO code and for helpful discussions.

Keywords: {3d–4f} SMMs · ab initio calculations · CASSCF calculations · density functional calculations · magnetic properties · {Ni_3-Ln} complexes · {Ni-Ln} SMMs

[1] a) R. Sessoli, D. Gatteschi, A. Caneschi, M. A. Novak, *Nature* **1993**, *365*, 141 – 143; b) D. N. Woodruff, R. E. P. Winpenny, R. A. Layfield, *Chem. Rev.* **2013**, *113*, 5110 – 5148.

[2] a) M. Affronte, *J. Mater. Chem.* **2009**, *19*, 1731 – 1737; b) A. Ardavan, O. Rival, J. J. L. Morton, S. J. Blundell, A. M. Tyryshkin, G. A. Timco, R. E. P. Winpenny, *Phys. Rev. Lett.* **2007**, *98*, 057201; c) L. Bogani, W. Wernsdorfer, *Nat. Mater.* **2008**, *7*, 179 – 186; d) A. Candini, S. Klyatskaya, M. Ruben, W. Wernsdorfer, M. Affronte, *Nano Lett.* **2011**, *11*, 2634 – 2639; e) M. N. Leuenberger, D. Loss, *Nature* **2001**, *410*, 789 – 793; f) A. R. Rocha, V. M. Garcia-Suarez, S. W. Bailey, C. J. Lambert, J. Ferrer, S. Sanvito, *Nat. Mater.* **2005**, *4*, 335 – 339.

[3] a) J. D. Rinehart, J. R. Long, *Chem. Sci.* **2011**, *2*, 2078 – 2085; b) L. Rosado Piquer, E. C. Sanudo, *Dalton Trans.* **2015**, *44*, 8771 – 8780.

[4] a) C. R. Ganivet, B. Ballesteros, G. de La Torre, J. M. Clemente-Juan, E. Coronado, T. Torres, *Chem. Eur. J.* **2013**, *19*, 1457 – 1465; b) R. J. Blagg, L. Ungur, F. Tuna, J. Speak, P. Comar, D. Collison, W. Wernsdorfer, E. J. L. McInnes, L. F. Chibotaru, R. E. P. Winpenny, *Nat. Chem.* **2013**, *5*, 673 – 678.

[5] a) W. Wernsdorfer, N. Aliaga-Alcalde, D. N. Hendrickson, G. Christou, *Nature* **2002**, *416*, 406 – 409; b) Y. N. Guo, G. F. Xu, W. Wernsdorfer, L. Ungur, Y. Guo, J. K. Tang, H. J. Zhang, L. F. Chibotaru, A. K. Powell, *J. Am. Chem. Soc.* **2011**, *133*, 11948 – 11951; c) F. Habib, P. H. Lin, J. Long, I. Korobkov, W. Wernsdorfer, M. Murugesu, *J. Am. Chem. Soc.* **2011**, *133*, 8830 – 8833.

[6] a) J. D. Rinehart, M. Fang, W. J. Evans, J. R. Long, *J. Am. Chem. Soc.* **2011**, *133*, 14236 – 14239; b) J. D. Rinehart, M. Fang, W. J. Evans, J. R. Long, *Nat. Chem.* **2011**, *3*, 538 – 542.

[7] T. Rajeshkumar, G. Rajaraman, *Chem. Commun.* **2012**, *48*, 7856 – 7858.

[8] T. Gupta, T. Rajeshkumar, G. Rajaraman, *Phys. Chem. Chem. Phys.* **2014**, *16*, 14568 – 14577.

[9] S. K. Langley, D. P. Wielechowski, V. Vieru, N. F. Chilton, B. Moubaraki, B. F. Abrahams, L. F. Chibotaru, K. S. Murray, *Angew. Chem. Int. Ed.* **2013**, *52*, 12014 – 12019; *Angew. Chem.* **2013**, *125*, 12236 – 12241.

[10] J. L. Liu, J. Y. Wu, Y. C. Chen, V. Mereacre, A. K. Powell, L. Ungur, L. F. Chibotaru, X. M. Chen, M. L. Tong, *Angew. Chem. Int. Ed.* **2014**, *53*, 12966 – 12970; *Angew. Chem.* **2014**, *126*, 13180 – 13184.

[11] a) V. Baskar, K. Gopal, M. Helliwell, F. Tuna, W. Wernsdorfer, R. E. P. Winpenny, *Dalton Trans.* **2010**, *39*, 4747 – 4750; b) M. Holynska, D. Premuzic, I. R. Jeon, W. Wernsdorfer, R. Clerac, S. Dehnen, *Chem. Eur. J.* **2011**, *17*, 9605 – 9610; c) S. K. Langley, N. F. Chilton, L. Ungur, B. Moubaraki, L. F. Chibotaru, K. S. Murray, *Inorg. Chem.* **2012**, *51*, 11873 – 11881; d) S. K. Langley, L. Ungur, N. F. Chilton, B. Moubaraki, L. F. Chibotaru, K. S. Murray, *Inorg. Chem.* **2014**, *53*, 4303 – 4315; e) S. K. Langley, D. P. Wielechowski, V. Vieru, N. F. Chilton, B. Moubaraki, L. F. Chibotaru, K. S. Murray, *Chem. Sci.* **2014**, *5*, 3246 – 3256; f) K. C. Mondal, G. E. Kostakis, Y. H. Lan, W. Wernsdorfer, C. E. Anson, A. K. Powell, *Inorg. Chem.* **2011**, *50*, 11604 – 11611; g) K. C. Mondal, A. Sundt, Y. H. Lan, G. E. Kostakis, O. Waldmann, L. Ungur, L. F. Chibotaru, C. E. Anson, A. K. Powell, *Angew. Chem. Int. Ed.* **2012**, *51*, 7550 – 7554; *Angew. Chem.* **2012**, *124*, 7668 – 7672; h) C. Papatriantafyllopoulou, W. Wernsdorfer, K. A. Abboud, G. Christou, *Inorg. Chem.* **2011**, *50*, 421 – 423.

[12] a) L. Ungur, M. Thewissen, J. P. Costes, W. Wernsdorfer, L. F. Chibotaru, *Inorg. Chem.* **2013**, *52*, 6328 – 6337; b) A. Borta, E. Jeanneau, Y. Chumakov, D. Luneau, L. Ungur, L. F. Chibotaru, W. Wernsdorfer, *New J. Chem.* **2011**, *35*, 1270 – 1279.

[13] a) F. Neese, *J. Am. Chem. Soc.* **2006**, *128*, 10213 – 10222; b) L. F. Chibotaru, L. Ungur, *J. Chem. Phys.* **2012**, *137*, 064112 – 064122; c) S. K. Singh, G. Rajaraman, *Chem. Eur. J.* **2014**, *20*, 113 – 123; d) S. K. Singh, G. Rajaraman, *Chem. Eur. J.* **2014**, *20*, 5214 – 5218; e) L. F. Chibotaru, L. Ungur, *Phys. Rev. Lett.* **2012**, *109*, 246403.

[14] a) S. K. Singh, T. Gupta, G. Rajaraman, *Inorg. Chem.* **2014**, *53*, 10835 – 10845; b) S. K. Singh, T. Gupta, M. Shanmugam, G. Rajaraman, *Chem. Commun.* **2014**, *50*, 15513 – 15516; c) S. K. Singh, N. K. Tibrewal, G. Rajaraman, *Dalton Trans.* **2011**, *40*, 10897 – 10906.

[15] a) V. Chandrasekhar, S. Das, A. Dey, S. Hossain, S. Kundu, E. Colacio, *Eur. J. Inorg. Chem.* **2014**, *2014*, 397 – 406; b) V. Chandrasekhar, B. M. Pandian, R. Boomishankar, A. Steiner, J. J. Viftal, A. Houri, R. Clerac, *Inorg. Chem.* **2008**, *47*, 4918 – 4929; c) T. Shiga, N. Ito, A. Hidaka, H. Ohkawa, S. Kitagawa, M. Ohba, *Inorg. Chem.* **2007**, *46*, 3492 – 3501; d) T. Shiga, H. Okawa, S. Kitagawa, M. Ohba, *J. Am. Chem. Soc.* **2006**, *128*, 16426 – 16427; e) T. Yamaguchi, J. P. Costes, Y. Kishima, M. Kojima, Y. Sunatsuki, N. Brefuel, J. P. Tuchagues, L. Vendier, W. Wernsdorfer, *Inorg. Chem.* **2010**, *49*, 9125 – 9135.

[16] a) C. G. Efthymiou, T. C. Stamatatos, C. Papatriantafyllopoulou, A. J. Tasiopoulos, W. Wernsdorfer, S. P. Perlepes, G. Christou, *Inorg. Chem.* **2010**, *49*, 9737 – 9739; b) N. F. Chilton, S. K. Langley, B. Moubaraki, K. S. Murray, *Chem. Commun.* **2010**, *46*, 7787 – 7789.

[17] J. P. Costes, S. Shova, J. M. Clemente Juan, N. Suet, *Dalton Trans.* **2005**, 2830 – 2832.

[18] a) S. K. Singh, G. Rajaraman, *Dalton Trans.* **2013**, *42*, 3623 – 3630; b) T. Rajeshkumar, H. V. Annadata, M. Evangelisti, S. K. Langley, N. F. Chilton, K. S. Murray, G. Rajaraman, *Inorg. Chem.* **2015**, *54*, 1661 – 1670.

[19] E. Ruiz, S. Alvarez, A. Rodriguez-Fortea, P. Alemany, Y. Pouillon, C. Massobrio, in *Magnetism: Molecules to Materials II: Molecule-Based Materials, Vol. 110* (Eds.: J. S. Miller, M. Drillon), Wiley-VCH, Weinheim, **2001**, pp. 227 – 280.

[20] L. Noodleman, *J. Chem. Phys.* **1981**, *74*, 5737 – 5743.

[21] a) E. Ruiz, G. Rajaraman, S. Alvarez, B. Gillon, J. Stride, R. Clerac, J. Larionova, S. Decurtins, *Angew. Chem. Int. Ed.* **2005**, *44*, 2711 – 2715; *Angew. Chem.* **2005**, *117*, 2771 – 2775; b) D. M. Low, G. Rajaraman, M. Helliwell, G. Timco, S. J. van, R. Sessoli, S. T. Ochsenbein, R. Bircher, C. Dobe, O. Waldmann, H.-U. Gudel, M. A. Adams, E. Ruiz, S. Alvarez, E. J. L. McInnes, *Chem. Eur. J.* **2006**, *12*, 1385 – 1396; c) G. Rajaraman, E. Ruiz, J. Cano, S. Alvarez, *Chem. Phys. Lett.* **2005**, *415*, 6 – 9; d) F. Neese, *Coord. Chem. Rev.* **2009**, *253*, 526 – 563; e) ref. [14c]; f) M. Atanasov, P. Comba, S. Hausberg, B. Martin, *Coord. Chem. Rev.* **2009**, *253*, 2306 – 2314; g) M. Atanasov, P. Comba, C. A. Daul, *Inorg. Chem.* **2008**, *47*, 2449 – 2463; h) M. Atanasov, C. Busche, P. Comba, H. F. El, B. Martin, G. Rajaraman, S. J. van, H. Wadepohl, *Inorg. Chem.* **2008**, *47*, 8112 – 8125; i) E. Cremades, S. Gomez-Coca, D. Aravena, S. Alvarez, E. Ruiz, *J. Am. Chem. Soc.* **2012**, *134*, 10532 – 10542.

[22] E. Ruiz, J. Cano, S. Alvarez, P. Alemany, *J. Comput. Chem.* **1999**, *20*, 1391 – 1400.

[23] Gaussian 09, Revision A.02, M. J. Frisch, G. W. Trucks, H. B. Schlegel, G. E. Scuseria, M. A. Robb, J. R. Cheeseman, G. Scalmani, V. Barone, B. Mennucci, G. A. Petersson, H. Nakatsuji, M. Caricato, X. Li, H. P. Hratchian, A. F. Izmaylov, J. Bloino, G. Zheng, J. L. Sonnenberg, M. Hada, M. Ehara, K. Toyota, R. Fukuda, J. Hasegawa, M. Ishida, T. Nakajima, Y. Honda, O. Kitao, H. Nakai, T. Vreven, J. A. Montgomery Jr., J. E. Peralta, F. Ogliaro, M. J. Bearpark, J. Heyd, E. N. Brothers, K. N. Kudin, V. N. Staroverov, R. Kobayashi, J. Normand, K. Raghavachari, A. P. Rendell, J. C. Burant, S. S.

Iyengar, J. Tomasi, M. Cossi, N. Rega, N. J. Millam, M. Klene, J. E. Knox, J. B. Cross, V. Bakken, C. Adamo, J. Jaramillo, R. Gomperts, R. E. Stratmann, O. Yazyev, A. J. Austin, R. Cammi, C. Pomelli, J. W. Ochterski, R. L. Martin, K. Morokuma, V. G. Zakrzewski, G. A. Voth, P. Salvador, J. J. Dannenberg, S. Dapprich, A. D. Daniels, Ö. Farkas, J. B. Foresman, J. V. Ortiz, J. Cioslowski, D. J. Fox, Gaussian, Inc., Wallingford, CT, USA, **2009**.

[24] A. D. Becke, *J. Chem. Phys.* **1993**, *98*, 5648 – 5652.

[25] T. R. Cundari, W. J. Stevens, *J. Chem. Phys.* **1993**, *98*, 5555 – 5565.

[26] A. Schäfer, C. Huber, R. Ahlrichs, *J. Chem. Phys.* **1994**, *100*, 5829 – 5835.

[27] a) M. M. Francl, W. J. Pietro, W. J. Hehre, J. S. Binkley, M. S. Gordon, D. J. Defrees, J. A. Pople, *J. Chem. Phys.* **1982**, *77*, 3654 – 3665; b) Pc. Hariharan, J. A. Pople, *Theor. Chim. Acta* **1973**, *28*, 213 – 222.

[28] J. Cirera, E. Ruiz, *CR Chim.* **2008**, *11*, 1227 – 1234.

[29] F. Aquilante, T. B. Pedersen, V. Veryazov, R. Lindh, *WIREs Comput. Mol. Sci.* **2013**, *3*, 143 – 149.

[30] K. Bernot, J. Luzon, L. Bogani, M. Etienne, C. Sangregorio, M. Shanmugam, A. Caneschi, R. Sessoli, D. Gatteschi, *J. Am. Chem. Soc.* **2009**, *131*, 5573 – 5579.

[31] S. K. Singh, T. Gupta, L. Ungur, G. Rajaraman, *Chem. Eur. J.* **2015**, *21*, 13812 – 13819.

[32] L. Chibotaru, L. Ungur, *University of Leuven* **2006**.

[33] L. Ungur, L. F. Chibotaru, *Lanthanides and Actinides in Molecular Magnetism*, Wiley-VCH, Weinheim, **2015**, Chapter 6, pp. 153 – 184.

[34] M. E. Lines, *J. Chem. Phys.* **1971**, *55*, 2977.

[35] A. N. Georgopoulou, R. Adam, C. P. Raptopoulou, V. Psycharis, R. Ballesteros, B. Abarca, A. K. Boudalis, *Dalton Trans.* **2010**, *39*, 5020 – 5027.

[36] S. K. Singh, T. Gupta, P. Badkur, G. Rajaraman, *Chem. Eur. J.* **2014**, *20*, 10305 – 10313.

[37] M. Pinsky, D. Avnir, *Inorg. Chem.* **1998**, *37*, 5575 – 5582.

[38] S. N. König, N. F. Chilton, C. Maichle-Mossmer, E. M. Pineda, T. Pugh, R. Anwander, R. A. Layfield, *Dalton Trans.* **2014**, *43*, 3035 – 3038.

[39] N. F. Chilton, D. Collison, E. J. L. McInnes, R. E. P. Winpenny, A. Soncini, *Nat. Commun.* **2013**, *4*, DOI: 10.1038/ncomms3551.

[40] L. Ungur, L. F. Chibotaru, *Phys. Chem. Chem. Phys.* **2011**, *13*, 20086 – 20090.

[41] J. L. Liu, Y. C. Chen, Y. Z. Zheng, W. Q. Lin, L. Ungur, W. Wernsdorfer, L. F. Chibotaru, M. L. Tong, *Chem. Sci.* **2013**, *4*, 3310 – 3316.

Received: August 6, 2015
Published online on November 23, 2015

